Microstructure and tensile properties of injection molded thermoplastic polyurethane with different melt temperatures

Ning Xiang,[1] Xiaowen Zhang,[1] Mengyao Zheng,[1] Yong Ge,[1] Tao Wang,[1] Haibao Liu,[2] Chris Maharaj,[3] John P. Dear,[2] Yue Yan[1]

[1]Beijing Institute of Aeronautical Materials, AECC, Beijing Engineering Research Centre of Advanced Structural Transparencies forthe Modern Traffic System, Beijing 100095, China

[2]Department of Mechanical Engineering, Imperial College London, London SW7 2AZ, United Kingdom

[3]Department of Mechanical and Manufacturing Engineering, The University of the West Indies, St. Augustine, Trinidad and Tobago
Correspondence to: Y. Yan (E-mail: yue.yan@biam.ac.cn) and X. Zhang (E-mail: wendy511@bit.edu.cn)

ABSTRACT: The use of injection molding technology to prepare heterogeneous interlayer film of laminated glass holds strong applicable potential. This article aims to investigate the effects of melt temperature and melt flow on the microstructure evolution and tensile properties of thermoplastic polyurethane (TPU) specimens during the injection molding process. The tensile properties of the TPU specimens show dependency on the melt temperature and melt flow direction. The results of birefringence indicate that melt flow and lower melt temperature induce higher stretching deformation of the molecular chain network. Small-angle X-ray scattering analysis approves that besides the melt temperature and flow direction, the testing position on the cross section of the specimen has great influence on the microstructure of the TPU sheet. Further analysis and conclusions can be made using wide-angle X-ray scattering method. The above results demonstrate that both the tensile properties and microstructure of the injection molded TPU specimens tend to be isotropic with the increase of melt temperature. © 2020 Wiley Periodicals, Inc. J. Appl. Polym. Sci. **2020**, *137*, 48891.

KEYWORDS: injection molding; structure-property relationships; thermoplastic polyurethane; X-ray

INTRODUCTION

Thermoplastic polyurethane (TPU) has been widely used in many engineering fields due to its advanced properties, including modulable flexibility, relatively higher strength, excellent elasticity, good abrasion resistance, and transparency.[1–3] As an interlayer, TPU can absorb impact energy, prevent penetration and glass fragments from splashing, thereby improving the structural strength and service life of the windshield. And compared with extrusion molding, which can only produce sheets, injection molding can realize the integral molding of interlayer with large curvature and large thickness. It is a new method for preparing interlayers.

TPU is a typical block copolymer synthesized by diisocyanate, polyester/polyether polyol, and small molecular chain extender.[4] Diisocyanate and chain extender form a hard segment that determines the melt temperature and high temperature properties of the material, while the soft segment is composed of long-chain polyols that mainly affect the low temperature properties and elasticity of the material.[5] Due to the poor compatibility of the soft and hard segments and the crystallization of the segments, the TPU block copolymers are separated into microphases or domains. In addition to the polymerization process, the processing also has a significant influence on the microstructure of the TPU, in turn, affects its mechanical properties.[6–9]

The change in melt temperature and the shear forces generated by the injection melt flow lead to the diversified distribution of the microphase within the material. Therefore, for block copolymers, the relationship between microscopic morphology, mechanical properties, and processing conditions becomes significant research interests. When the material is heated beyond the melt temperature of the hard segments, a homogeneous viscous melt would be created and the microphase separation structure disappears. After cooling, the domain structure can be reconstructed.[10]

The earliest literature on the mechanical behavior of polyurethanes focuses on the relationship between modulus and temperature. It is assumed that the hard phase in the glass state is the filler and the continuous phase of the soft segment acts as the matrix.[11–14] In recent years, more related research has been completed by many researchers. Frick and Mikoszek[15] studied the influence of melting conditions on the structural evolution and mechanical properties of aromatic polyurethanes by injection

molding. The induced behavior of the molding process was studied using light microscopy, scanning electron microscopy, and differential scanning calorimeter (DSC). As the melt temperature increased, the observed crystals, from the optical microscopic results, decreased and the tensile deformation increased. Through DSC analysis, it was found that there was diversity of crystalline structures along the change of the melt temperature during injection molding. Small-angle X-ray scattering (SAXS) and wide-angle X-ray scattering (WAXS) were successfully used to characterize the structure on the nanometer and sub-nanometer scale. The dimension of the soft and hard segments in the TPU molecular chain is nanoscale, which can be monitored by SAXS. As early as 1983, Koberstein studied the domain structure and the boundary thickness between the hard and soft domains using the SAXS and DSC techniques.[16,17] Blundell *et al.*[18] used real-time SAXS technology to determine the evolution of the microstructure of TPUs with different morphology micrographs during tensile deformation, and explored the mechanism of structural changes during deformation. The experimental results showed that when the hard blocks were randomly dispersed, the hard phase regions were separated from each other in an affine manner during the stretching process and did not affect each other. When the hard blocks were monodispersed, the hard phase interacted to prevented affine deformation of the structure. Moreover, Stribeck *et al.*[19] studied the effect of melt temperature on the structure and mechanical properties of TPUs. SAXS results showed hard domains were only affected by the neighboring structures. Therefore, another model, which was called "sandwich," was developed to explain the nonaffine deformation of nanostructure during stretching process. The authors pointed out that the "sandwich" microstructures containing the shorter soft segments between hard segments featured a strain limit under high tensile deformation. And with the melt temperature rose, mechanical properties of material declined. Zhao *et al.*[20–22] studied the relationship between the mechanical response of styrenic block copolymers and the melt temperature of injection molding. Meanwhile, the influence of shear stress field on the microstructure by employing dynamic pressure-preserving injection molding technology was studied.

The analysis of the rheological properties of TPU provides a good correlation with the microstructure. Therefore, the study of the rheological properties of TPU can be a useful method to analysis and understand the structures. Yamasaki *et al.*[23] investigated the effects of the molecular aggregation structure on the rheological properties of TPU and found that the formation of well-organized hard segment domains had a profound effect on the rheological properties of TPU. Lu *et al.*[24] studied the rheological properties of TPU at small and large deformation via three different types of rheometry: dynamic shear, capillary, and torque. It was proved that the abnormally high flow activation energy of TPU was caused the contributions of flow and the degradation reaction. Yoon *et al.*[25] studied the effect of thermal history on the rheological behavior of TPU. It was found that melt temperature employed for specimen molded had a profound influence on the variations of the dynamic storage and loss moduli with time.

Most of the existing research focus on the mechanism of the action of melt temperature on phase structure and performance during injection. However, no systematic study highlights the mechanical anisotropy as function of melt temperature and melt flow during TPU injection molding. In this study, a series of TPU sheets have been prepared by using injection molding with different melt temperatures. The tensile properties were analyzed in different directions. In particular, the microscopic morphology of different scales was characterized by diverse analytical techniques, such as birefringence, DSC, SAXS, and WAXS. The effects of melt temperature and melt flow on both tensile properties and microstructure evolution at different scales of TPU specimens have been investigated. An attempt to analyze the relationship between the mechanical anisotropy and microstructure has also been made.

EXPERIMENTAL

Materials

The polymer under investigation was TPU AG8451 from Lubrizol Advanced Materials. The melt flow index is 13.18 g/10 min at 190 °C with the poise weight of 2.16 kg according to ASTM D1238-2004.[26] The shore A hardness is 70A and density is 1.08 g cm^{-3} according to the technical data sheet.

Preparation of Specimens

The TPU sheets were molded using a 130-ton injection molding machine CX 130-750 of Krauss-Maffei, Germany. The TPU pellets were fully dried under hot wind at 80 °C after 6 h. The size of the molded TPU sheets was 200 mm in length, 100 mm in width, and 3 mm in thickness. As shown in Tables I and II, the sheets were prepared at different melt temperatures while keeping other processing parameters invariable.

Measurement and Characterizations

Tensile Properties Testing. The measurement of the tensile properties of the injection molded TPU sheets were performed on a GT-AI3000 (GOTECH Testing Machines Inc.) in accordance with ISO 37:2005.[27] As shown in Figure 1, Type 1A dumbbell-shaped specimens, which were cut in two different directions on the plate according to ISO 37:2005, were selected for the experiments. In those two directions, one is parallel to the direction of melt flow, marked as PF, and the other one is perpendicular to the direction of melt flow, marked as VF. The initial distance between the clamps was 20 mm and separated speed of the grips is 500 mm s^{-1}. The engineering stress, $\sigma = F/A_0$, is computed from the force, F, measured by the load cell, and A_0 is the initial central cross section of the specimen. The engineering tensile strain ε equals to $(l\text{-}l_0)/l_0$, where l_0 = 20 mm is the distance between the initial displacement extensometer fixture, and l is the actual distance between the extensometer fixture.

Birefringence Measurement. Birefringence is a particular property of the transparent polymers, which is caused by material anisotropy. Thus, isotropic solids do not exhibit birefringence.

Table I. Melt Temperature in the Experiment

Factor	Level 1	Level 2	Level 3
Melt temperature (°C)	160	170	180

Table II. Basic Processing Parameters of Injection Molding

Processing parameters	Value
Mold temperature (°C)	30
Injection volume (cm^3)	71.5
Injection speed (mm s^{-1})	3
Cooling time (s)	60

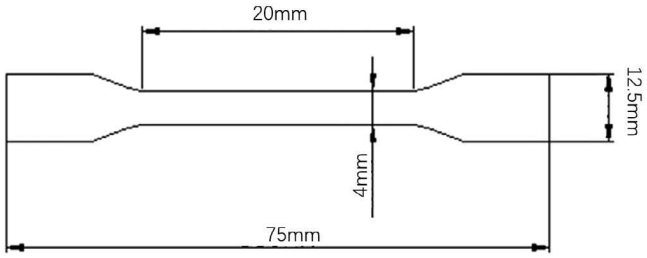

Figure 1. Geometry of dumbbell-shaped TPU specimen.

The molecular formation is "frozen" into a stretched conformation when the TPU melt is filled into the cold mold. The material exhibits anisotropy and thus birefringence occurs. The birefringence (Δn) can be reflected by the optical path difference (OPD), which is defined as[28]:

$$\Delta n = \Gamma / d \tag{1}$$

where Γ is the measured optical retardation, which is also called as OPD and d is the thickness of slices.

A polarized optical microscope (WPA-100-L; Photonic Lattice Inc., Japan) was used to measure the OPD of TPU slices, which were cut from the injection molded sheets in two directions, which are parallel and perpendicular to the direction of the melt flow, respectively. These TPU slices have a width of 2.2 mm, shown in Figure 2.

Differential Scanning Calorimetry. DSC studies were carried out on a DSC25 (TA Instruments) machine. About 5 mg injection molded TPU sheets were used for the DSC measurements, which were conducted at a temperature range of −80 to 250 °C with a heating rate of 10 K min^{-1}. First, lower the temperature to −80 °C and keeping the isothermal condition for 5 min, then raising the temperature to 250 °C. During the measurements, the specimens are protected using nitrogen flux to avoid heating degradation.

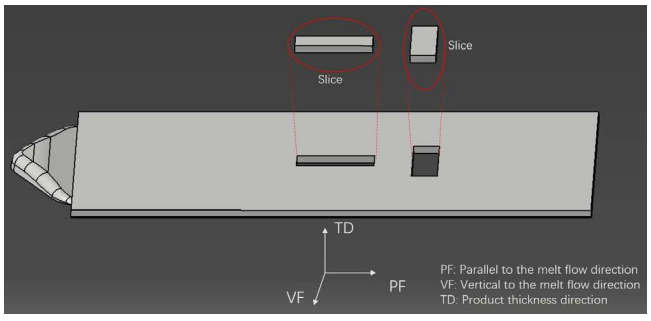

Figure 2. Schematic diagram of the orientation of the test slice relative to the part. [Color figure can be viewed at wileyonlinelibrary.com]

Small-Angle X-ray Scattering. SAXS measurements were carried out using a Bruker Nano STAR camera. The specimens used for SAXS testing had the same dimensions as those for the birefringence measurement. In this study, the structural differences were compared between specimens at processing temperatures of 160 and 180 °C, respectively. The SAXS properties in the through-width direction of the specimens were obtained and four locations were selected for the SAXS measurements as shown in Figure 3. The experiments were conducted in both the parallel and perpendicular directions to the melt flow. The distance between the specimen and the detector was 1070 mm, offering a scattering angle range of 0.1–3.6°. Scattering patterns were collected by Vantec 2000 detector. The collimation, specimen chamber, and flight tube before the detector were evacuated to minimize air scattering. The scattering time is 1800 s.

Wide-Angle X-ray Scattering. WAXS measurements were performed using a Bruker Nano STAR camera. The distance between the specimen and the detector was 47 mm, to offer a scattering angle range of 3–40°, and the scattering time is 1800 s. Data collection was identical to that for the SAXS experiments and the locations of inspection points were kept the same as the SAXS experiments. In this way, the Herman's factor which can be calculated by eqs. (2) and (3) over the azimuthal angle range from 0 to 180°, was used to represents the degree of molecular orientation,[29–33] given by:

$$f_{or} = \frac{3 < \cos^2\phi > -1}{2} \tag{2}$$

$$< \cos^2\phi > = \frac{\int_0^{\pi/2} I(\phi)\cos^2\phi \sin\phi d\phi}{\int_0^{\pi/2} I(\phi)\sin\phi d\phi} \tag{3}$$

where f_{or} is the Herman's factor. When polymer chains are completely arranged along the reference direction, f_{or} = −0.5. When polymer chains are random coil, f_{or} = 0. In the above equation, ϕ is the azimuth angle and $I(\phi)$ is the scattering intensity at angle ϕ. $<\cos^2\phi>$ is an average orientation factor.

Rheological Properties. The shear viscosity of the TPU pellets, which were dried under hot wind at 80 °C for 6 h was measured as a function of shear rate using a dual barrel capillary rheometer (Rosand RH2000; Malvern Panalytical Ltd., UK) at constant temperature. The testing temperatures were 160, 170, and 180 °C, respectively. The shear rate range was from 20 to 6000 s^{-1}, and 10 data points were collected for each test. The diameter of the die was 1 mm and the aspect ratio was 16:1.

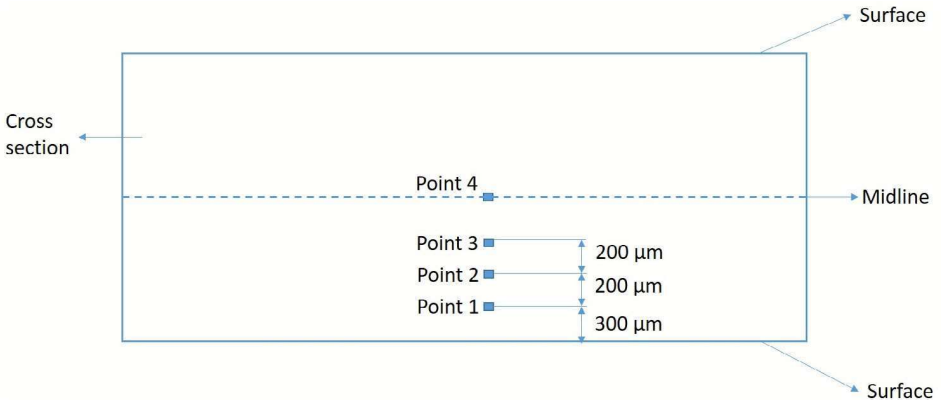

Figure 3. Schematic diagram of location selection of SAXS measurement. [Color figure can be viewed at wileyonlinelibrary.com]

RESULTS AND DISCUSSION

Tensile Properties

The stress-strain curves of the TPU specimens which were manufactured using injection molding at different melt temperatures are shown in Figure 4. It can be found that the uniaxial tensile curves of TPU specimens were characterized as no yielding point and presented a large strain at break values. Except the specimen that molded at the melt temperature of 160 °C and cut along the melt flow direction, the others exhibited a viscohyperelastic behavior[34] under the uniaxial tension. This is because small agglomerations of hard segments in matrix as incompatible individual islands or percolated network is the important factor for the deformation behavior at strain regime and can lead to viscoelastic behavior of TPU.[35] During initial loading stage, the soft phase between the hard domains are stretched and deformed[36] while the hard phase remained unstained. With the continued stretching, the molecular chain extension in the soft phase will be continued, and the molecular chain network begins to deform. The hard domains start to carry stress and constrain the extension of the molecular chain and the deformation of the molecular chain network, during which the stress increase slowly with the tensile strain. At this stage, the hard domains play an important role in the entity of the stress, acting as a sort of rigid filler in the soft matrix. Some hard domains are destructed during deformation. With increasing strain, the molecular chain networks are reoriented. Meanwhile, strong hard domains begin to deform under the high stress. At this stage, the stress rises sharply as the strain increases until the specimen is fractured.

When the melt temperature was 160 °C, the stress–strain behavior in the PF direction did not show a strain-hardening phenomenon and demonstrated a higher stress value at the beginning of the stretch than those other conditions, this might be caused by the special microstructure of the TPU specimen. As shown in Figure 5, when the melt temperature was 160 °C, the shear viscosity of the pellets was higher than that of 170 and 180 °C, indicating that harder melt flow at the same shear rate. Therefore, the melt flow during injection at 160 °C causes the higher orientation of the molecular segments and more serious stretching of the molecular chain network along the flow direction than those in the VF direction. The molecular segments seem to be prestretched, which results in a higher tensile stress at the beginning of the loading process in the PF direction while the lower elongation at break than that in the VF direction. It is previously found that the hard domains are oriented perpendicular to the melt-flow direction during injection molding.[19] This may explain why the strain-hardening phenomena were only presented in the VF direction under high strain when the specimens were formed at 160 °C.

On the other hand, the orientation of the molecular segments and the deformation of the molecular chain networks would be frozen more easily for the samples molded at 160 than 170 and 180 °C. The reason is that the melt will be cooled more quickly, for the 160 °C melt temperature, after touched the mold. Therefore, as the melt temperature rose, the difference in tensile properties of the specimens in both directions decreased and both exhibited a visco-hyperelastic behavior. Further structural analysis had been carried out in the following sections using the birefringence, SAXS, and WAXS measurements.

Figure 6 reveals the tensile mechanical data of the TPU at different melt temperatures. It is observed that at lower melt temperatures, there was a great deviation in the tensile strength and elongation at break values in the two directions. The directionality features with respect to molecular chain orientation and molecular chain network deformation thus appear to be reduced with the rising melt temperature. It can also be found from Figure 6(c,d) that the tensile stress at a given elongation decreased as the melt temperature rose, which might be caused by the destruction of the strong hard domains. And the number of strong hard domains was characterized by DSC.

Thermal Properties

The heat flow traces of the raw material and the injection molded sheets obtained using the DSC measurement are shown in Figure 7. Only the curves between 50 and 250 °C are displayed. The first reason is that curves mainly characterized the glass transition process of the soft segment at temperature range of −80 to 50 °C and the curves are featureless. The second is to highlight the influence of the melt temperature on the regularity of the hard domains. The peak values of the curves in Figure 7 are shown in Table III. It was noted that the pellets had two endothermic peaks during the heating process. It has been known that the microphase separation of TPU can make the soft and hard

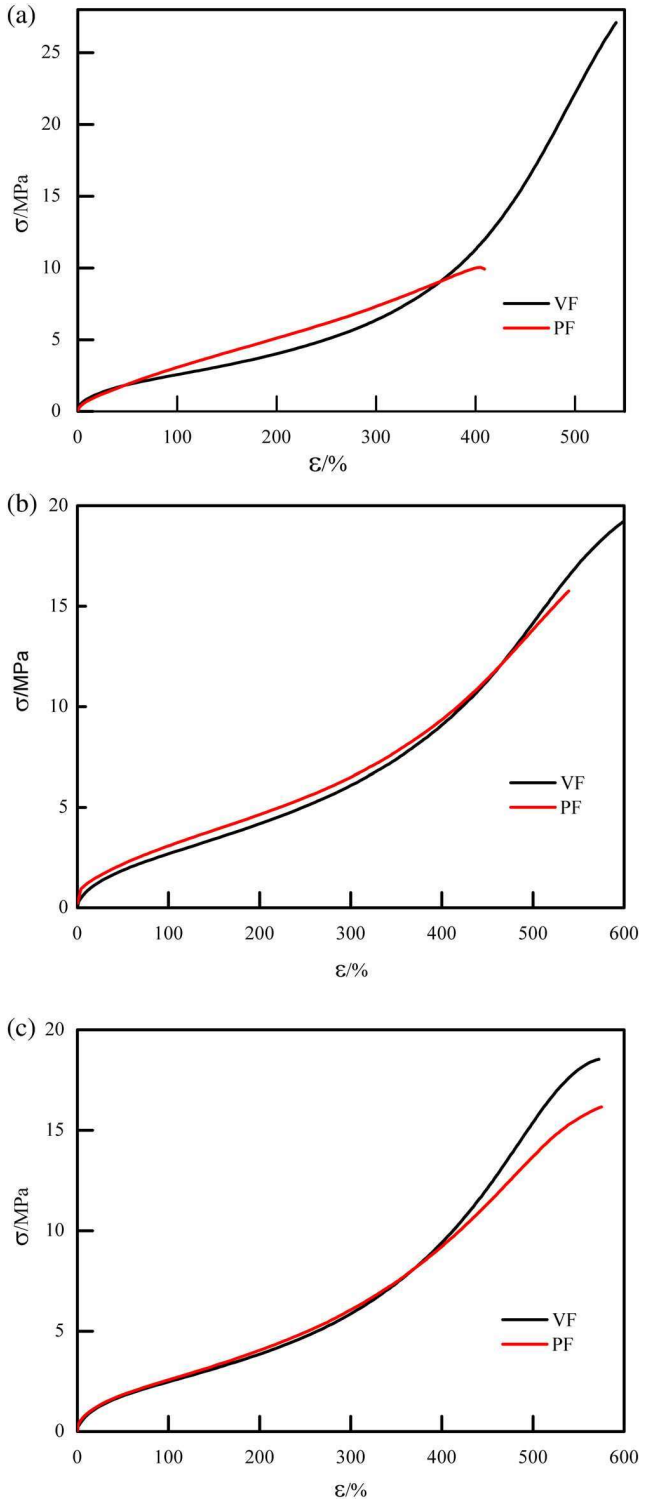

Figure 4. The stress-strain curves of the TPU specimens molded at different melt temperatures. (a) 160 °C, (b) 170 °C, (c) 180 °C. VF means the tensile direction is perpendicular to the melt flow direction and PF means that parallel to the melt flow direction. [Color figure can be viewed at wileyonlinelibrary.com]

segments inside the material agglomerate to form two phases. Thus, it consists of hard domains in a soft-domain matrix and the hard domains themselves contain both hard segments and soft segments. The peak at temperature about 80 °C (Peak 1) was a phase transition endotherm, related to the short-range ordered structure of hard domains. And the peak at 209 °C (Peak 2) was the melting of the crystallites, which were merged with some proximate hard segments. The more microcrystals in the hard domains, the stronger hard domain will be. In addition, those crystallites are only quasi-crystalline rather than completely crystalline.[37] The main reason for this conclusion is that the endothermic peak temperature of TPU is relatively low.[37,38]

The specimen with the melt temperature of 160 °C still presented two endothermic peaks during the endothermic process, meaning that the specimen was phase separated in its morphology and the crystallites were retained. However, compared with the pellets, the intensity of Peak 2 was weakened, indicating that part of the crystallites was destroyed. As the melt temperature increased from 160 to 180 °C, Peak 2 disappeared due to the increased chain mobility, which can destroy the crystallites. Therefore, the decline and disappearance of Peak 2 indicate the reduction in the number of crystallites. After the processing, the temperature of Peak 1 was lower than that of pellets and the Peak 1 shifted from 78 to 75 °C with the increase of the melt temperature. The hard domains appear to be lost with increasing melt temperature. Meanwhile, due to the low temperature of the mold surface and the rapid cooling of sheets after filling, it is difficult to form a stable short-range ordered structure. Therefore, the temperatures of the Peak 1 presented by the injection molded sheets were reduced. It indicates that the microphase separation structure of the melt is removed as the melt temperature increased. Combining with the previous analysis, the reduction of the number of strong hard domains and the destruction of the microphase separation structure are the main reason for the general decrease of tensile stress at a given elongation with melt temperature increased, as shown in Figure 6(c,d).

Birefringence Results

The OPD distribution of TPU specimens is shown in Figure 8, which can give some information on the conception of molecular chain network. As the width of different specimens are

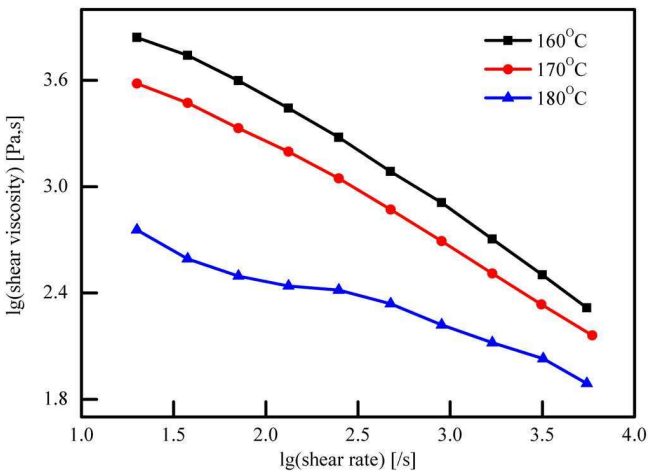

Figure 5. The shear viscosity VS shear rates plots for raw pellets at different temperatures. [Color figure can be viewed at wileyonlinelibrary.com]

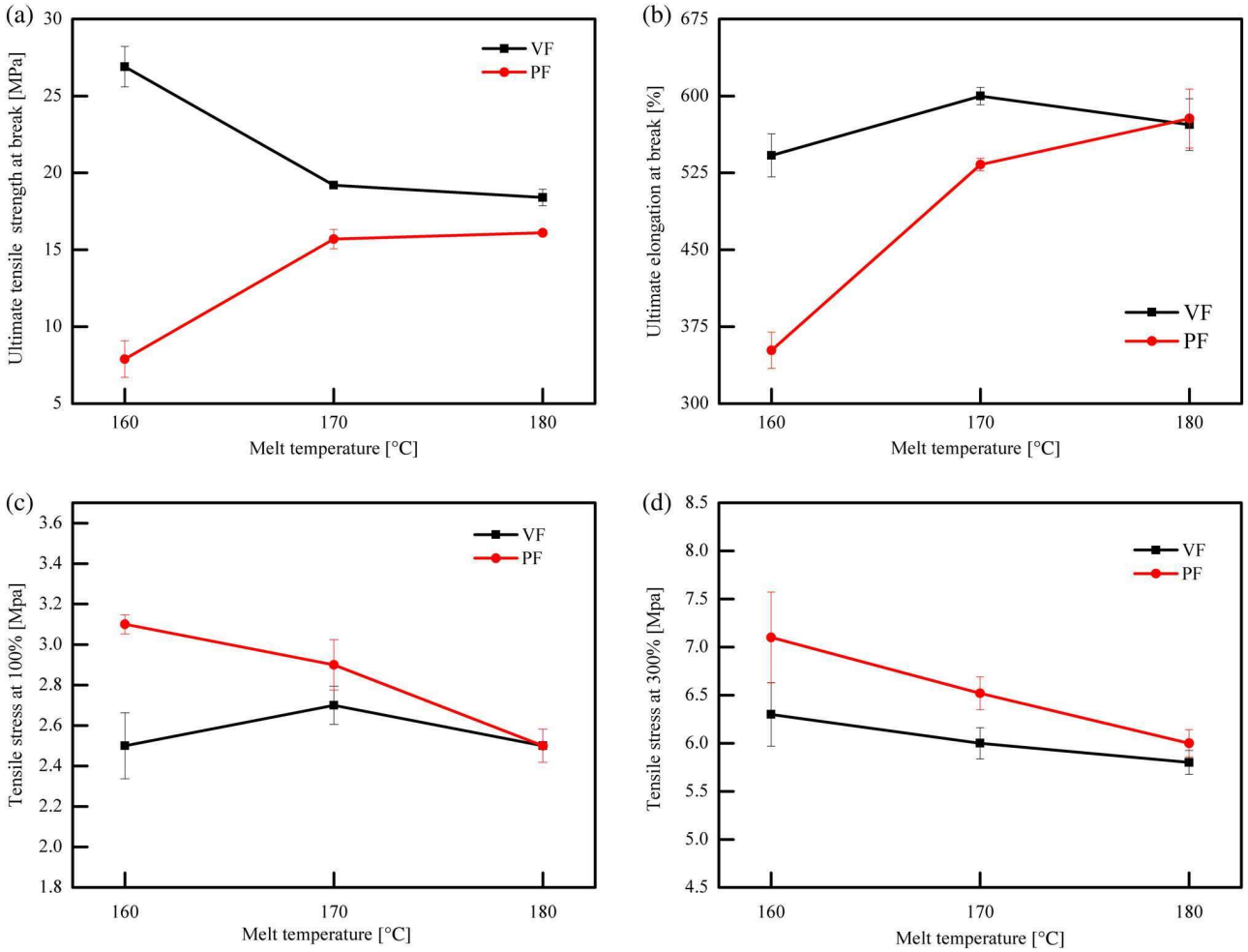

Figure 6. The tensile mechanical data of the TPU at different melt temperatures. (a) Ultimate tensile strength at break, (b) ultimate elongation at break, (c) tensile stress at 100% elongation, (d) tensile stress at 300% elongation. VF means the tensile direction is perpendicular to the melt flow direction and PF means that parallel to the melt flow direction. [Color figure can be viewed at wileyonlinelibrary.com]

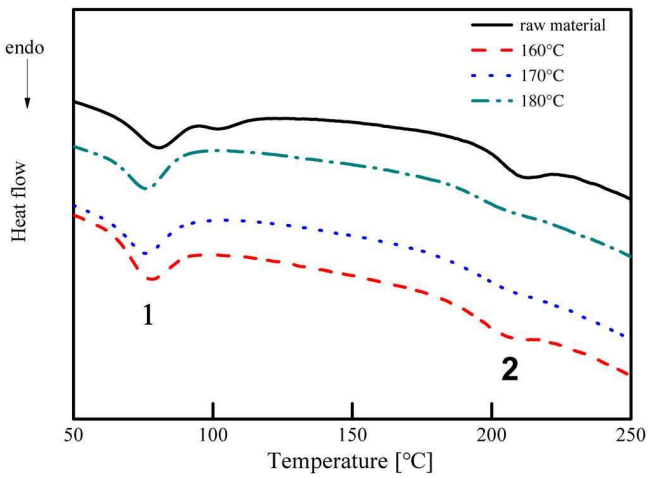

Figure 7. DSC traces of TPU material before (raw pellets) and after injection molding. The labels at the dashed curves indicate the temperature of the injection melt. [Color figure can be viewed at wileyonlinelibrary.com]

approximately the same, the difference in the distribution of optical path is caused by the different microphase structures. In Figure 8(a,b), when the melt temperature was 160 °C, the OPD values of the TPU slices along the direction of the melt flow were much higher than that in the VF direction. This means that the overall molecular chain network undergoes more seriously stretching deformation along the flow direction during the filling and cooling process, which led to the anisotropy of the TPU specimens. However, when the melt temperature increased to 180 °C, the discrepancy of the OPD values in both directions decreased because the higher melt temperature accelerated the relaxation of the molecular chain network. The stretching deformation limits the deformation of the mesh chain during stretching in the melt flow direction, resulting in a decrease in elongation at break. It can also better explain the tensile properties discussed in Tensile Properties section.

The OPD values in the horizontal centerline of the different specimens are shown in Figure 9. Similar conclusions can be drawn as discussed above, with the increasing melt temperature, the

Table III. Melt Temperature, T_m and Melt Enthalpies, ΔH_m from the DSC Scans. The Processed Materials Are Labeled with the Melt Temperature

	Peak 1		Peak 2	
Specimen	T_m (°C)	ΔH_m (J g^{-1})	T_m (°C)	ΔH_m (J g^{-1})
Raw material	80	1.76	209	1.32
160 °C	78	3.34	206	0.96
170 °C	76	3.28	—	
180 °C	75	2.94	—	

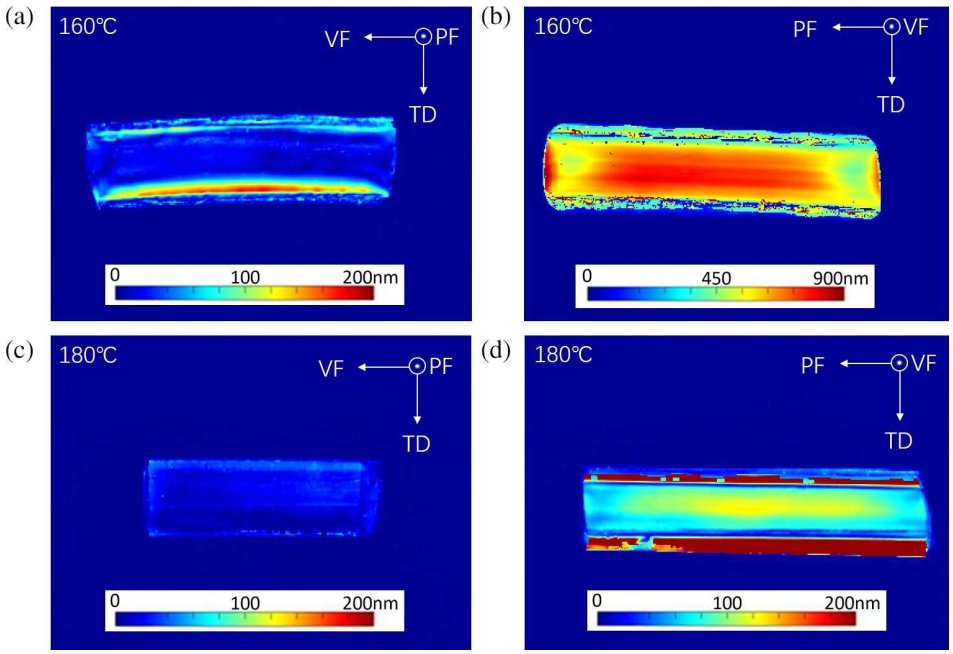

Figure 8. The OPD distribution of the injection molded TPU specimens with the melt temperature of 160 and 180 °C, respectively. In (b) and (d), the specimen was cut in the direction of the melt flow, and in (a) and (c), the cutting route was perpendicular to the melt flow direction. [Color figure can be viewed at wileyonlinelibrary.com]

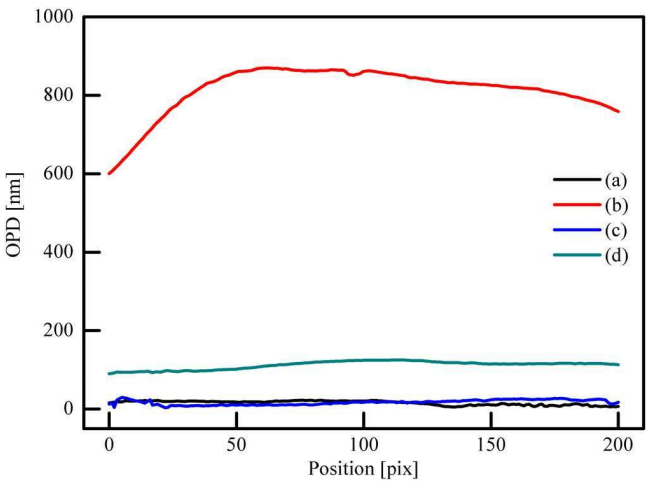

Figure 9. The OPD distribution curve of the specimen on the horizontal center line. The solid lines (a–d) are corresponded to Figure 8(a–d), respectively. [Color figure can be viewed at wileyonlinelibrary.com]

value of OPD decreased significantly in the PF direction, while in the VF direction, the value of OPD was small with a little change. It further illustrates that the stretching deformation of the molecular chain network, in the PF direction, has been mainly caused by the melt flow. All the above phenomena can be further validated by the WAXS results.

SAXS Results

To better observe the structural features with relatively low degree of molecular orientation, the q *VS* $I(q)q^2$ curves, which are also named the Lorentz correction curves, of the injection molded TPU specimens have been obtained through the original two-dimensional–SAXS patterns as shown in Figure 10. q is a scattering vector, defined: $q = (4\pi/\lambda) \sin\theta$. The parameter λ is the wavelength and θ is the scattering angle. Some scholars have found that, the long spacing, calculated from $I(q)$ *VS* q curves, is related to the extent of the phase separation when the specimen is heated. In the same range of temperatures as the hard segment melting, the long spacing disappearance showing that a

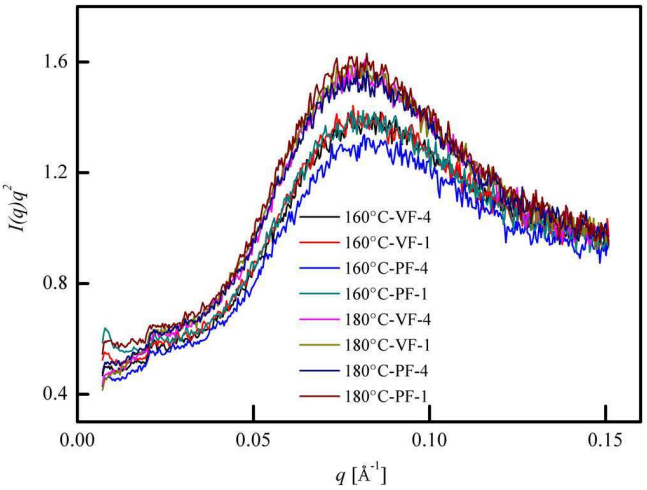

Figure 10. The q *VS* $I(q)q^2$ curves of the injection molded TPU specimens with the melt temperature of 160 and 180 °C, respectively. VF means vertical direction to the melt flow while PF is parallel direction. The Numbers 1 and 4 indicate the position of the test point. [Color figure can be viewed at wileyonlinelibrary.com]

homogeneous melt is produced by melting.[39] Therefore, the Lorentz correction curves can also be used to characterize the phase separation.

The peaks in the curve represented the relative position between the hard domains. The long spacing, which means the distance between the hard domains, can be calculated using eq. (4) according to the position of the Bragg peak. If the long spacing increases, the size of the hard domains will increase. The reason is that the relative proportion of the soft and hard segments does not change during the processing. It can be seen from Figure 10 that the Bragg peaks of different specimens were coincident with about 8 nm, which means that different molding temperatures had no effect on the distance between the hard domains. The long spacing between different specimens is consistent, indicating that the hard segment agglomerates in the specimen generally have the same size.

$$d_{\mathrm{Bragg}} = 2\mathrm{n}/q_{\mathrm{peak}}(\mathrm{nm}) \tag{4}$$

Figure 11 shows intensity VS azimuthal angle curves corresponding to the Points 1 and 4 for the injection molded TPU specimens with the melt temperature of 160 and 180 °C, respectively. The position of testing Point 1 was close to the surface layer while the position of testing Point 4 was near to the center of the cross section. The orientation of the domains can be characterized by the azimuth integration calculation of the two-dimensional patterns. From the azimuthal angle curves, the full-width at half-maximum (FWHM) of the azimuth integral curve between 0 and 180° can be calculated, the degree of orientation (Π) of different testing positions can be defined as Π = (180-FWHM)/180. The corresponding results are shown in Table IV. It can be concluded that both the melt temperature and the distance from the testing point to the surface have influence on the orientation degree of the hard domains.

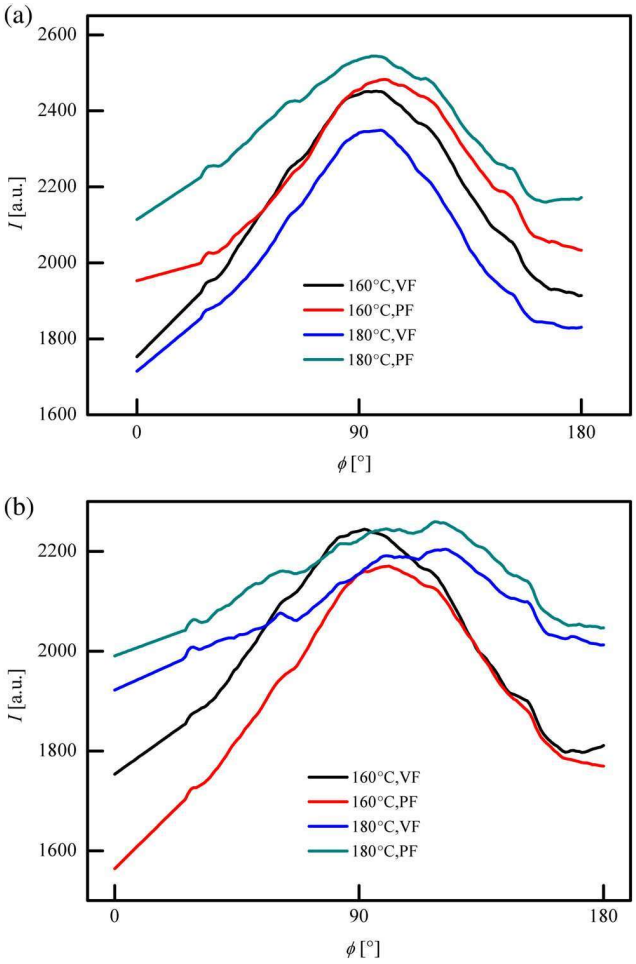

Figure 11. The intensity VS azimuthal angle curves of testing point one and four with the melt temperature of 160 and 180 °C, respectively. (a) Testing Point 1 and (b) testing Point 4. VF means spline cutting direction is perpendicular to the melt flow direction and PF means spline cutting direction parallel to the melt flow direction. [Color figure can be viewed at wileyonlinelibrary.com]

It has been found from Figure 11 and Table IV that the hard domains presented more reorientation in the surface layer rather than the core layer, independent of melt temperature. This can

Table IV. The FWHM and the Degree of Orientation (Π) of the Different Specimens

Specimen	FWHM	Π
160 °C - VF - 1	48	0.74
160 °C - PF - 1	42	0.77
180 °C - VF - 1	51	0.71
180 °C - PF - 1	53	0.70
160 °C - VF - 4	50	0.72
160 °C - PF - 4	69	0.67
180 °C - VF - 4	63	0.65
180 °C - PF - 4	56	0.68

be explained as the surface layer of the specimens cools faster after the melt contact with the surface of the mold and more hard domains have been maintained. However, more time will be permitted for the movement of the molecular segment since the core layer cools slower, inducing lower orientation degree of the hard domains. In the surface region, the orientation of the hard domains decreased as the melt temperature rose, due to that the higher melt temperature benefits to the free movement of the molecular segment.

Besides, Table IV shows that the value of Π was 0.72 in the VF direction at the core region, which was larger than that in the PF direction when melt temperature was 160 °C. However, as the melt temperature increased to 180 °C, the value of Π decreased significantly and became similar in the two directions. The results indicate that the orientation degree of the hard domains in the VF direction is greater than that in the other direction when the melt temperature is relatively low. Other studies[19] have also drawn similar conclusions that the hard domain in a TPU injection molded part would be reoriented to the perpendicular direction to the melt-flow direction. This is also expected, when the melt temperature is 160 °C, the hard domains are not destroyed completely based on the DSC results. As a result, some stronger hard domains can be reserved and oriented in the VF direction. Therefore, in the VF direction, the strong hard domains can be better stressed to greatly increase the strength in the late stage of tensile stretching. This illustrates the phenomena that the specimens formed at 160 °C have the strain-hardening phenomena only in the VF direction under high strain. When the melt temperature is 180 °C, the microphase separation structure disappears completely and the orientation direction of the hard domains is no longer obvious. As a result, the specimen formed at 180 °C shows the strain-hardening phenomena in the two directions and the tensile strength at break decreases.

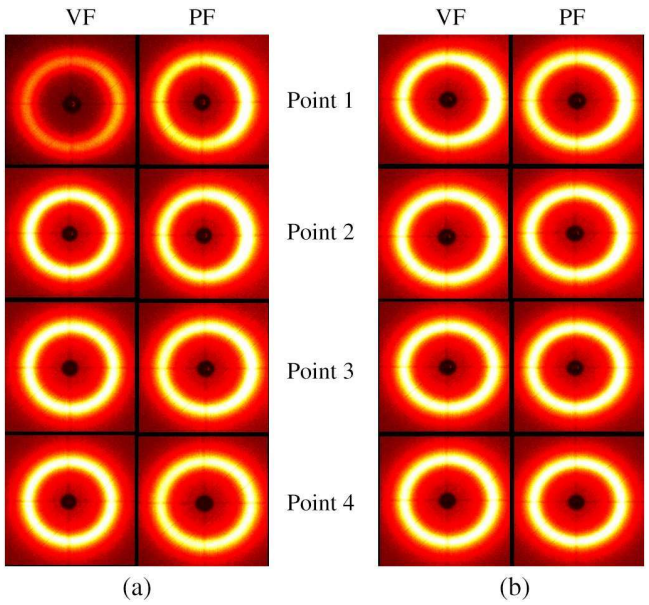

Figure 12. The WAXS patterns of TPU slices in the different positions of the cross section. (a) The specimen that molded at 160 °C and (b) the specimen that molded at 180 °C. VF means spline cutting direction is perpendicular to the melt flow direction and PF means spline cutting direction parallel to the melt flow direction. Numbers 1–4 indicate the testing point. [Color figure can be viewed at wileyonlinelibrary.com]

WAXS Results

To exhibit more microscopic structural information of the injection molded specimens, the WAXS patterns, obtained from different positions of the cross section with different melt temperatures, are shown in Figure 12. The amorphous halo in the WAXS results probed the orientation of the inter chain gaps, which was perpendicular to the chain axis. The direction of the amorphous halo meridian was perpendicular to the long side of the spline. In Figure 12, it was found that the amorphous halo of testing Points 1 and 2, near the surface, exhibited a certain degree of asymmetric structure, indicating that the microstructure within the specimen exhibited anisotropy. As the testing point approached to the core layer, the amorphous halo appeared almost isotropic.

Figure 13 displays the corresponding inclinational slices through the maximum of the amorphous halo, and the background scattering in the pattern has been subtracted. The curves describe the orientation of the molecular segments. From Figure 13, it can be intuitively found that the molecular chain orientation was significantly different in the PF and VF directions when the melt temperature was 160 °C. At the position of the testing Points 1 and 2, there was a clear molecular segment orientation in the PF direction. However, only at the position of testing point 1 in the VF direction, slightly oriented molecular chain was referred by the WAXS intensity of the surface layer, while subsurface layer did not change with azimuth. When the melt temperature raised to 180 °C, the degree of the molecular chain orientation was similar in both directions, and only the molecular chains were oriented at testing Points 1 and 2.

In order to quantitatively describe this orientation degree, the Herman's factor, $f_{or}(P)$, had been calculated from Figure 13 as a function of the testing point (P) and the results have been shown in Figure 14. From the testing Points 1 to 4, the Herman's factor increased to nearly zero, indicating that the orientation degree of the molecular chains was lowered from the surface layer to the core layer. It also can be seen from Figure 14 that when the melt temperature was 160 °C, the difference in the value of the Herman's factor was obvious at testing point of 2 and 3. f_{or} (2) and f_{or} (3) of specimen molded at 160 °C in the PF direction were −0.031 and −0.013, respectively. However, for specimen molded at 160 °C in the VF direction, both f_{or} (2) and f_{or} (3) were close to zero. It indicates that the molecular chain is oriented along the melt flow direction, caused by the orientation of the chain segment in the PF direction, and this orientation is preserved due to the relatively lower melt temperature. This conclusion is corresponding to the results of the birefringence because the molecular segment orientation and the stretch deformation of the molecular chain network are both caused by melt flow and cooling freezing. Therefore, at lower melt temperature, the orientation of the molecular segments is directional, which cause a decrease in elongation at break and an increase in tensile stress under small strain along the flow direction. Due to the influence of low mold temperature, the orientation degree of molecular

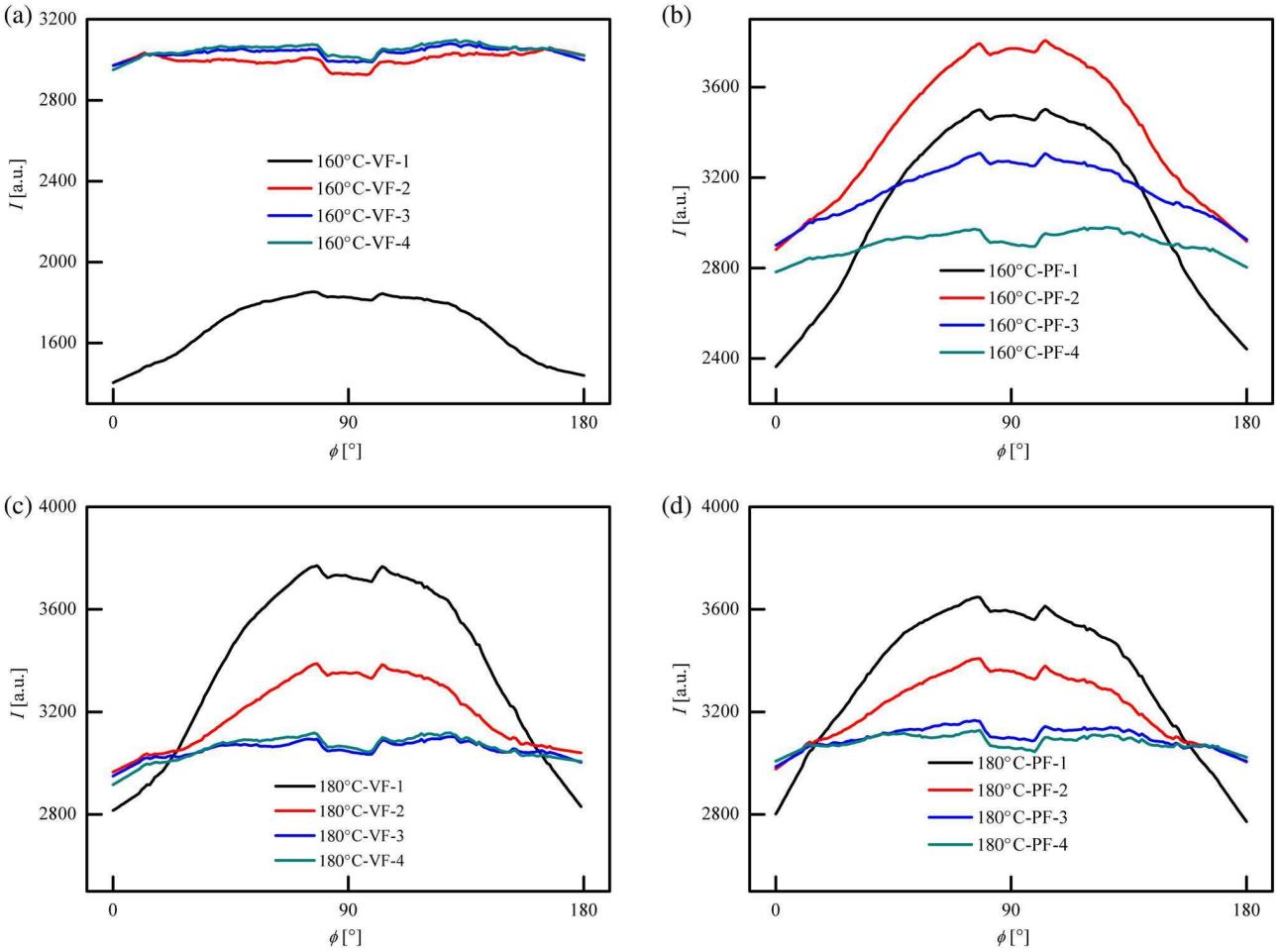

Figure 13. The WAXS intensity in the pole figure cut through the maximum of the amorphous halo with the melt temperature of 160 and 180 °C, respectively. ϕ = 0 is on the meridian. VF means spline cutting direction is perpendicular to the melt flow direction and PF means spline cutting direction parallel to the melt flow direction. Numbers 1–4 indicate the testing point. [Color figure can be viewed at wileyonlinelibrary.com]

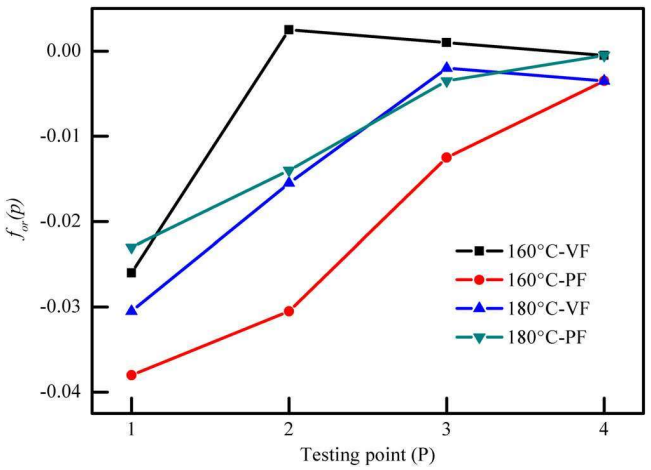

Figure 14. The Herman's factor, $f_{or}(P)$ which computed from Figure 13 with the melt temperature of 160 and 180 °C, respectively. VF means vertical direction to the melt flow while PF is parallel direction. [Color figure can be viewed at wileyonlinelibrary.com]

chain segment in the surface layer was the largest, and the core layer melt was rearranged in the cooling stage due to its relatively slower cooling rate. Therefore, the results showed that f_{or} (1) was the smallest and f_{or} (4) was near to zero. When the melt temperature was 180 °C, the orientation degree of the molecular chain was similar in both PF and VF direction at all testing points except the Point 1. This may due to the higher melt temperature facilitates the molecular segment rearrangement of the core layer, therefore, the orientation of the molecular chain in the core layer was weakened and the $f_{or}(P)$ values became almost the same for the testing points of 3 and 4.

Evolution Model of Microstructure

Through the characterization and analysis of the microstructure of TPU at different scales, the mechanism of the melt temperature influence on the microstructure was clarified, and the corresponding model was established as shown in Figure 15. Due to the higher viscosity of the melt at 160 °C, the higher shear force would like to induce higher molecular chain orientation along the melt flow direction than that obtained at 180 °C, as shown in Figure 15(a,d). The molecular chain orientation has

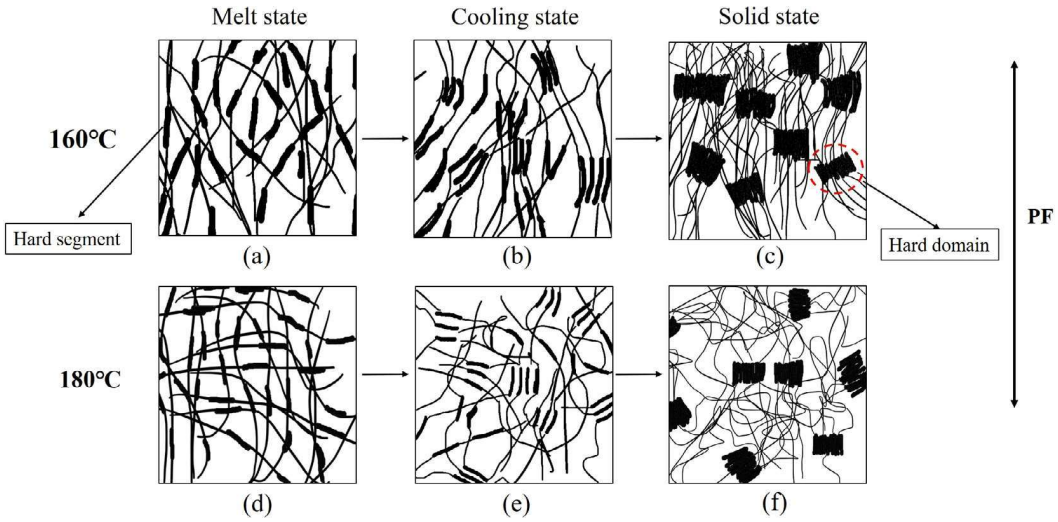

Figure 15. Schematic picture of the structure development of the TPU molded at different melt temperature. (a–c) The structure development process at the melt temperature of 160 °C, and (d–f) the structure development process at the melt temperature of 180 °C. PF means parallel to the melt flow direction. [Color figure can be viewed at wileyonlinelibrary.com]

mostly been frozen during the cooling stage of the melt when the melt temperature is 160 °C while some relaxation would happen for the melt temperature of 180 °C proved by the birefringence and WAXS results, as shown in Figure 15(b,e). This is because the higher viscosity and lower melt temperature make the free movement of molecular chain difficult at lower melt temperature. As the temperature decreases, the compatibility of the soft segment and the hard segment decreases and the hard segments begin to agglomerate into hard domains under the action of intermolecular force and hydrogen bond force. Finally, a relatively stable microphase separation structure is formed. According to the theory of fold-chain fringed micellar grain model, the molecular chains in the ordered region are arranged approximately parallel. Therefore, the hard domains are oriented along the VF direction because the molecular chains are arranged along the direction of melt flow, as shown in Figure 15(c), which can be confirmed by the SAXS results. Due to the relaxation of the molecular chain and chain segment when melt temperature is 180 °C, the orientation arrangement of the hard domains and the stretching deformation of the molecular chain network are no longer obvious, as shown in Figure 15(f), corresponding to the results of the birefringence and SAXS.

CONCLUSIONS

This article investigated the effects of melting temperature on the microstructure and tensile properties of TPU sheet after injection molding process. Through a systematic study, the effect of melt temperature and melt flow direction on the tensile properties and microstructure was measured and analyzed. The following conclusions can be drawn:

1. The tensile properties of the TPU specimens exhibit anisotropy with the melt temperature of 160 °C. In parallel direction of melt flow, the specimen does not show a visco-hyperelastic behavior, but the tensile stress at given elongation is higher than that in other directions. However, in the vertical direction, the tensile strength and ultimate elongation at break are higher, and the strain-hardening phenomena are observed. As the melt temperature increased, the tensile properties tend to be consistent in both directions.
2. The molecular chain network undergoes deformation in parallel to the direction of melt flow proved by the results of birefringence. When the melt temperature is 160 °C, the large stretching deformation of the molecular chain network causes a great difference in the elongation at break in two directions, which is opposite to 180 °C melt temperature.
3. The results of SAXS and WAXS further explain under the 160 °C melt temperature, the oriented molecular segments in the melt flow direction results in the higher the tensile stress at given elongation, and the higher orientation of hard domains in the perpendicular direction to the flow direction caused the strain-hardening phenomena. As the melt temperature increased, the microstructure of specimens tends to be isotropic, which corresponds to the change of tensile properties. The results also prove that the injection molded samples have a distinct skin-core structure and TPU molecules near the surface layer orient higher than the core layer.

REFERENCES

1. Sánchez-Adsuar, M. S.; Papon, E.; Villenave, J. *J. Appl. Polym. Sci.* **2000**, *76*, 1596.
2. Jose, S.; Li, J.; Bouzidi, L.; Leao, A. L.; Narine, S. S. *Polymer.* **2014**, *55*, 6764.
3. Charlon, M.; Heinrich, B.; Matter, Y.; Couzigné, E.; Donnio, B.; Avérous, L. *Eur. Polym. J.* **2014**, *61*, 197.
4. Bartolomé, L.; Aurrekoetxea, J.; Urchegui, M. A.; Tato, W. *Mater. Des.* **2013**, *49*, 974.
5. Kull, K. L.; Bass, R. W.; Craft, G.; Julien, T.; Marangon, E.; Marrouat, C.; Harmon, J. P. *Eur. Polym. J.* **2015**, *71*, 510.

6. Elwell, M. J.; Mortimer, S.; Ryan, A. J.; Bras, W. *Nucl. Instrum. Methods Phys. Res.* **1995**, *97*, 261.
7. Pompe, G.; Pohlers, A.; Pötschke, P.; Pionteck, J. *Polymer.* **1998**, *39*, 5147.
8. Lombardo, L.; Arreghini, A.; Maccarrone, R.; Bianchi, A.; Scalia, S.; Siciliani, G. *Prog. Orthod.* **2015**, *16*, 41.
9. Frick, A.; Mikoszek, M. *Macromol Symp.* **2010**, *294*, 102.
10. Datta, J.; Kasprzyk, P. *Polym. Eng. Sci.* **2017**, *58*, E14.
11. Cooper, S. L.; Tobolsky, A. V. *J. Appl. Polym. Sci.* **2010**, *10*, 1837.
12. Estes, G. M.; Cooper, S. L.; Tobolsky, A. V. *J. Macromol. Sci. Part C.* **1970**, *4*, 54.
13. Seymour, R. W.; Cooper, S. L. *Macromolecules.* **1973**, *6*, 48.
14. Huh, D. S.; Cooper, S. L. *Polym. Eng. Sci.* **1971**, *11*, 369.
15. Frick, A.; Mikoszek, M. *Macromol. Symp.* **2012**, *311*, 57.
16. Koberstein, J.; Stein, R. S. *Journal of Polym. Sci. Part B: Polym. Phys.* **1983**, *21*, 1439.
17. Leung, L. M.; Koberstein, J. T. *J. Polym. Sci.: Polym. Phys. Ed.* **1985**, *23*, 1883.
18. Blundell, D. J.; Eeckhaut, G.; Fuller, W.; Mahendrasingam, A.; Martin, C. *Polymer.* **2002**, *43*, 5197.
19. Stribeck, N.; Zeinolebadi, A.; Sari, M. G.; Frick, A.; Mikoszek, M.; Botta, S. *Macromol. Chem. Phys.* **2011**, *212*, 2234.
20. Zhao, Y.; Ning, N.; Hu, X.; Li, Y.; Chen, F.; Fu, Q. *Polymer.* **2012**, *53*, 4310.
21. Zhao, Y.; Su, B.; Zhong, L.; Chen, F.; Fu, Q. *Ind. Eng. Chem. Res.* **2014**, *53*, 15287.
22. Zhao, Y.; Su, B.; Chen, F.; Fu, Q. *Soft Matter.* **2015**, *11*, 2300.
23. Yamasaki, S.; Nishiguchi, D.; Kojio, K.; Furukawa, M. *Polymer.* **2007**, *48*, 4793.
24. Lu, Q. W.; Hernandez-Hernandez, M. E.; Macosko, C. W. *Polymer.* **2003**, *44*, 3309.
25. Yoon, P. J.; Han, C. D. *Macromolecules.* **2000**, *33*, 2171.
26. ASTM Standard D1238-13. Standard Test Method for melt flow rates of thermoplastics by extrusion plastometer. ASTM Standard **2013**.
27. ISO37. Rubber, vulcanized or thermoplastic. Determination of Tensile Stress-Strain Properties; International Organization: Geneva, Switzerland, **2011**.
28. Wimberger-Friedl, R. *Prog. Polym. Sci.* **1995**, *20*, 369.
29. Liu, X.; Zheng, G.; Dai, K.; Jia, Z.; Li, S.; Liu, C. *J. Mater. Sci.* **2011**, *46*, 7830.
30. Liu, X.; Zheng, G.; Jia, Z.; Li, S.; Liu, C.; Zhang, Y. *J. Appl. Polym. Sci.* **2012**, *125*, 2297.
31. Liu, Z.; Liu, X.; Zheng, G.; Dai, K.; Liu, C.; Shen, C. *Polym. Test.* **2017**, *58*, 227.
32. Jia, C.; Zhang, Q.; Liao, X.; Zhu, J.; Wu, L.; Ni, K. *Polymer.* **2015**, *67*, 92.
33. Luo, F.; Liu, X.; Shao, C.; Zhang, J.; Shen, C.; Guo, Z. *Mater. Des.* **2018**, *144*, 25.
34. Yang, L. M.; Shim, V. P. W.; Lim, C. T. *Int. J. Impact Eng.* **2000**, *24*, 545.
35. Randall, D.; Lee, S. The Polyurethanes Book; John Wiley & Sons: New York, **2002**.
36. Ehrenstein, G. W. Polymeric Materials: Structure Properties-Applications; Hanser: Munich, Germany, **2012**.
37. Sonnenschein, M. F.; Lysenko, Z.; Brune, D. A.; Wendt, B. L.; Schrock, A. K. *Polymer.* **2005**, *46*, 10158.
38. Saiani, A.; Daunch, W. A.; Verbeke, H.; Leenslag, J. W.; Higgins, J. S. *Macromolecules.* **2001**, *34*, 9059.
39. Adem, E.; Angulo-Cervera, E.; González-Jiménez, A.; Valentín, J. L.; Marcos-Fernández, A. *Radiat. Phys. Chem.* **2015**, *112*, 61.